THE ASTROPHYSICAL JOURNAL, 404:294–304, 1993 February 10

RADIAL PULSATIONS IN DB WHITE DWARFS?

STEVEN D. KAWALER
Department of Physics and Astronomy, Iowa State University, Ames, IA 50011
Received 1992 April 28; accepted 1992 August 12

ABSTRACT

Theoretical models of DB white dwarfs are unstable against radial pulsation at effective temperatures near 20,000–30,000 K. Many high-overtone modes are unstable, with periods ranging from 12 s down to the acoustic cutoff period of approximately 0.1 s. The blue edge for radial instability lies at slightly higher effective temperatures than for nonradial pulsations, with the temperature of the blue edge dependent on the assumed efficiency of convection. Models with increased convective efficiency have radial blue edges that are increasingly closer to the nonradial blue edge; in all models the instability persists into the nonradial instability strip. Radial pulsations therefore may exist in the hottest DB stars that lie below the DB gap; the greatest chance for detection would be observations in the ultraviolet. These models also explain why searches for radial pulsations in DA white dwarfs have failed: the efficient convection needed to explain the blue edge for nonradial DA pulsation means that the radial instability strip is 1000 K cooler than found in previous investigations. The multiperiodic nature of the expected pulsations can be used to advantage to identify very low amplitude modes using the uniform spacing of the modes in frequency. This frequency spacing is a direct indicator of the mass of the star.

Subject headings: stars: oscillations — white dwarfs

1. INTRODUCTION

In any account of the history of stellar evolution white dwarf stars appear frequently as objects that provide key insights and understanding of stars and the physics which governs their structure. White dwarfs provided an early successful application of relativity and quantum mechanics, which was needed to understand their tiny radii and very high mean densities. In more recent times, the principles of stellar seismology have seen their most successful application in studies of the ZZ Ceti stars and other nonradially pulsating white dwarfs (Kawaler 1990; Winget 1988). Furthermore, such pulsation studies of white dwarfs hold great promise for probing the history of star formation in our Galaxy (Wood 1992).

One episode in this history has recently been revisited. Ledoux & Sauvenier-Goffin (1950) showed via a vibrational stability analysis that if white dwarfs derived their luminosity from hydrogen burning, they would be vibrationally unstable. The lack of observed brightness variations at that time led them to conclude that the energy source of white dwarfs must be something other than nuclear fusion. This work set the stage for Mestel's (1952) model of white dwarf cooling, with residual heat from prior evolutionary stages providing the stellar luminosity. Somewhat ironically, it turned out that some white dwarfs do indeed pulsate; the observed pulsations are very low amplitude nonradial pulsations. These pulsations, which occur in white dwarfs within three distinct regions in the H-R diagram, have proved to be extremely useful probes of the interiors of white dwarf stars. These multiperiodic pulsations allow us to determine the precise masses of these stars, to determine their rotation periods, to decode the compositional stratification of their outer layers, and to actually measure their evolutionary time scales (Kawaler 1990; Winget 1988).

The same theoretical tools that so successfully describe the nonradial pulsations of the ZZ Ceti stars and the pulsating DB white dwarfs make an as yet unconfirmed prediction. White dwarf stars near the ZZ Ceti instability strip are unstable to *radial pulsations* with periods between 0.1 and 10 s. These radial mode instabilities are driven by the $\kappa - \gamma$ mechanism operating in the outer hydrogen partial ionization zone. Many groups have discussed these radial mode instabilities (i.e., Starrfield, Cox, & Hodson 1979; Saio, Winget, & Robinson 1983; Starrfield et al. 1983; Starrfield & Cox 1989).

Unfortunately, observational searches to date have not found evidence for radial pulsations in DA white dwarfs (Robinson 1984). While it is possible that the current models are in error because of effects not included in the modeling (i.e., Starrfield & Cox 1989), it is also possible that the amplitude of the pulsations is below the current observed upper limits. Ground-based searches for radial pulsations in DA white dwarfs are limited by the small number of photons (necessitating long runs) as well as the noise introduced into the data by the Earth's atmosphere (i.e., scintillation noise and other short-period transparency variations). In an ideal world, these observations would be performed from space, where scintillation is nonexistent, and using a sufficiently large telescope so that photon statistics do not hide periodic signals in short runs. Such a facility currently exists as the *Hubble Space Telescope* at least during the time that the High Speed Photometer remains on board. In part because of the capabilities of the *HST* for ultraviolet observations, it can observe white dwarfs at significantly higher photon count rates than from the ground.

Prior studies of radial pulsations in white dwarfs have concentrated on the hydrogen-envelope DA stars. To date, no systematic study of the radial pulsation properties of DB white dwarf models has been published, although individual models are discussed in Cox et al. (1987) and Starrfield & Cox (1989). Such stars, with effective temperatures of 25,000 to 30,000 K are more promising targets than the DA stars for study with *HST*. This paper presents a comprehensive theoretical analysis of the pulsation properties of DB white dwarfs at temperatures between 20,000 and 33,000 K. These objects are also found to be unstable against radial pulsations; this work characterizes the radial instability strip for these stars. Several interesting

properties of the radially unstable modes make them useful in their own right for seismological study of white dwarfs. In particular, the frequency spacing of high-overtone radial modes provides a very accurate mass determination for these stars. Section 2 describes the construction of the equilibrium models of white dwarfs used in the subsequent pulsation analysis and discusses the properties of the models relevant to their radial pulsation properties. The mechanics of the pulsation calculations are described in § 3. Sections 4 and 5 summarize the results of the adiabatic and nonadiabatic analysis, respectively, of the models. Observational searches, past and future, for radial pulsations in white dwarfs are discussed in the context of these new models in the concluding section.

2. MODELS

To explore radial pulsational instabilities in DB stars, we first constructed a grid of models of helium-envelope white dwarfs. Most models are 0.60 $M_\odot$, with a surface layer of 10^{-3} stellar masses of helium. For each of three convective efficiencies, we constructed models with effective temperatures between 19,000 and 32,000 K. The hottest models represent the hottest DB white dwarfs that lie at the base of the well-known gap in the DB luminosity function between about 30,000 K and 40,000 K. The structural properties of these models are very similar to the evolutionary models described by Tassoul, Fontaine, & Winget (1990).

Equilibrium models used in this study are part of a new series of white dwarf models designed for pulsation analysis. The models presented here are technically static envelope integrations, as they are not part of a stellar evolutionary sequence. Since most of the action in radial pulsations in classical variable stars occurs well above any luminosity sources, static envelopes such as these are quite adequate for linear radial pulsation calculations for the fluffy variables such as Cepheids, RR Lyra stars, and δ Scuti stars. However, in white dwarf stars, the eigenfunctions penetrate below the surface layers, and into regions of changing composition and luminosity. Hence static models for white dwarf pulsation studies must in general be more carefully constructed to be considered realistic. To be more specific, models of white dwarfs cannot assume constant luminosity with depth in all regions of interest; the models must extend more deeply into the core where energy is generated by residual gravitational contraction and release of stored thermal energy.

As long as there is no nuclear energy generation, neutrino cooling of the core is small, and residual gravitational contraction is a minor energy source, the energy generation rate for degenerate stellar material is proportional to the specific heat per unit mass and the rate of cooling of the core. If the core is isothermal, and sufficiently degenerate that only the ions contribute to the specific heat, then the energy generation rate per unit mass is a constant, proportional to the cooling rate (see Van Horn 1971). These conditions are all satisfied in the cool white dwarfs (Savedoff, Van Horn, & Vila 1969), so that these stars have luminosity profiles that can be accurately modeled by assuming that the luminosity within a shell of radius r is proportional to the mass contained within that shell. Indeed, this prescription has been used by many investigators as a short cut to white dwarf models with reasonable thermal profiles (i.e., Dziembowski & Koester 1981; Cox et al. 1987; Kawaler & Weiss 1990). While the variable DB white dwarfs are hotter than those studied by the above authors, their luminosity profiles can still be approximated by the above procedure. This procedure does ignore neutrino emission, which can be a contributing cooling effect in the hottest models. Examination of evolutionary sequences of 0.60 $M_\odot$ models shows that at $T_e = 30{,}000$ K, the neutrino luminosity is approximately 40% of the photon luminosity; the neutrino luminosity drops with decreasing effective temperature (Iben & Tutukov 1984).

With the above specification for the luminosity profile, we integrate the usual equations describing stellar structure from the surface to a point $0.001M_*$ from the center. We use a fourth-order Runge-Kutta integration scheme. The step size is controlled to limit roundoff and truncation errors and to maintain sufficient zoning resolution for the subsequent pulsation analysis. For overall accuracy of all quantities of 1 part in 10^6, this scheme results in models with approximately 300 shells. The step size was further reduced so that all models have approximately 600 zones stored, with the zoning criterion that fractional changes in the primary quantities remain smaller than 0.035 from one zone to the next. To obtain a model with a specified effective temperature, mass, and surface helium layer thickness, we adjusted the model luminosity to ensure that the density of the innermost point matched the mean density of the central ball. In this way, these envelope models are essentially complete stellar models.

Our models have almost pure helium envelopes surrounding homogeneous cores of 50% carbon, 50% oxygen by mass. By the time DB white dwarfs cool to the temperatures where radial instabilities occur, gravitational settling purifies the surface helium layers, with most heavy elements (in particular C and O) having settled below the envelope and into the degenerate core. The abundance profile of helium as a function of depth can therefore be closely approximated by assuming diffusive equilibrium throughout the model. With this assumption, the helium abundance with depth is determined using the diffusive equilibrium prescription described by Arcoragi & Fontaine (1980). For all of our models, we assume a helium layer mass of $0.001M_*$, based on recent seismological studies of PG 1159 (Kawaler & Bradley 1993). The pulsation results presented here are very insensitive to the surface helium layer thickness as long as the helium represents more than 10^{-10} stellar masses.

The equation of state used in the integrations is analytic throughout, but with a temperature switch to simulate the effects of pressure ionization. At temperatures below $10^{6.0}$ K we compute the density assuming an ideal, nondegenerate gas using the Saha equation for ionization equilibrium. At temperatures above $10^{6.2}$ K, we assume complete ionization and that the ions are nondegenerate. The electron pressure in this regime is computed using the algorithm described by Eggleton, Faulkner, & Flannery (1973), and Coulomb interactions between the ions is treated as in Iben & Tutukov (1984) and Koester & Schönberner (1986). Between $\log(T) = 6.0$ and $\log(T) = 6.2$, we interpolate linearly in $\log(T)$ between the fully ionized and Saha equations of state. The switch in the equation of state occurs well below the driving region for most modes and has no significant effect on the computed growth rates. Radiative opacities are taken from the Los Alamos Opacity Library using tables with compositions ($Y = 0.999$, $Z = 0.001$) and ($Y = 0$, $C = 0.999$, $Z = 0.001$). An additional H-rich table was used for the DA sequence described in § 6. Conductive opacities are computed using the Iben (1975) fit to the tables of Hubbard & Lampe (1969). All tabular interpolations use four-point Lagrangian interpolation in density

and temperature, and simple linear interpolation in composition. The equation of state and opacity computations are all designed to maximize the smoothness of the determined quantities and their derivative with respect to density and temperature. In the construction of the models we have reduced as much as possible the numerical noise in the models since it is amplified in the higher order pulsation calculations.

Convection is treated using variations of the classic Böhm-Vitense mixing length theory. We consider three cases of increasing convective efficiency. Using the terminology of Arcoragi & Fontaine (1980) (see also Tassoul et al. 1990) they are ML1, ML2, and ML3. Readers are urged to consult the above references for details. In short, ML1 is the classic treatment, ML2 is more efficient because of different assumptions about horizontal energy transport, and ML3 is the most efficient as it is the same as ML2 but with a mixing length to pressure scale height ratio of 2 instead of 1. In all cases, we also follow the practice of limiting the pressure scale height near the top of a convection zone (Böhm & Stuckl 1967) though this additional factor plays only a small role in the results of the computations.

A very important property of the equilibrium models is the thermal time scale at the base of the surface convection zone

$$\tau_{\rm bc} = \int_0^{q_{\rm bc}} \frac{c_v T}{L} M_* \, dq \,, \qquad (1)$$

where c_v is the specific heat, $q = (1 - M_r/M_*)$ is the fractional mass below the surface, and M_* is the mass of the model (Cox 1980). The subscript "bc" refers to quantities at the base of the convection zone; thus the integral proceeds from the surface to the base of the convection zone. For the driving of pulsations by partial ionization mechanisms, driving is most efficient when the thermal time scale in the partial ionization region matches the pulsation period of interest. Thus the time scale at the base of the surface convection zone is a key parameter for investigations of pulsational instability. The value of $\tau_{\rm bc}$ is shown in Figure 1 for the 0.60 $M_\odot$ ML1, ML2, and ML3 sequences of models. The values of $\tau_{\rm bc}$ found for the models in this study agree remarkably well with the results of Tassoul et al. (1990).

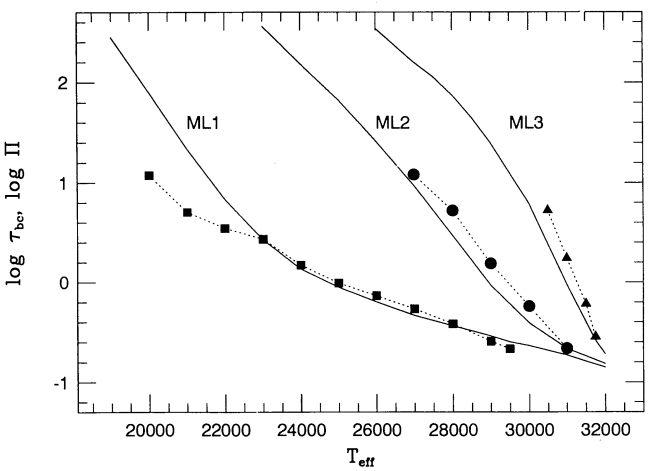

FIG. 1.—The thermal time scale at the base of the surface convection zone in DB white dwarf models, as compared with the longest period unstable radial mode. Solid curves show $\tau_{\rm bc}$ for model sequences with three different prescriptions for convection. Symbols connected by dotted lines show log Π for the longest period unstable mode for models at the given temperatures. All times and periods are in seconds.

By inspection of Figure 1, we can get a preview of the results to be presented later. As the convection zone base moves downward, the thermal time scale $\tau_{\rm bc}$ increases. The blue edge for radial instability should be near the effective temperature where $\tau_{\rm bc}$ is approximately equal to periods characteristic of high-overtone radial modes. Thus the blue edge for radial pulsations will be where $\tau_{\rm bc}$ is a few tenths of a second, i.e., at about 30,000 K, with a small dependence on the efficiency of convection. For comparison, the blue edge for nonradial g-mode oscillations will fall where $\tau_{\rm bc}$ is approximately equal to the lowest overtone g-mode period of about 100 s. This nonradial blue edge, first explored by Winget et al. (1983), lies at about 28,000 K for ML3 to 20,000 K for ML1 in our models.

3. RADIAL PULSATION COMPUTATIONS

3.1. *Adiabatic Oscillation Frequencies*

The equilibrium models described in the previous section were analyzed with two separate stellar oscillation codes. Our pulsation analysis is based on the equations described in Saio, Winget, & Robinson (1983, hereafter SWR). Those authors, who used a relaxation code to compute eigenfunctions and eigenvalues, noted the difficulty in fully resolving the eigenfunctions for high-overtone modes. As a result, their node count for a given eigenfrequency was necessarily ambiguous. To resolve the eigenfunctions fully and therefore obtain accurate oscillation frequencies, requires a very large number of zones in an equilibrium model when solving the equations with relaxation techniques.

To obtain accurate pulsation periods for the radial modes, we used a shooting technique to solve the differential equations describing linear, adiabatic radial oscillation (see, for example, Cox 1980). These equations relate the relative perturbations of the radius and pressure of a concentric spherical shell with the mechanical properties of the equilibrium model. The starting conditions for the inward integration were obtained using the surface boundary conditions: the first condition is the chosen normalization of the eigenfunctions, while the second condition ensures that the pressure is regular at the surface. Integration inward was performed using a fourth-order Runge-Kutta routine. To ensure that roundoff and truncation error were minimized, the Runge-Kutta steps were subject to quality control using the techniques described by Press et al. (1986). To obtain the coefficients of the differential equations between shells of the model, we interpolated all equilibrium model quantities using bicubic splines. The effective number of shells used ranged from 50 shells for low-order overtones to 20,000 shells for the highest overtone modes computed. The results of the adiabatic computations were therefore very insensitive to the number of shells in the equilibrium model. Increasing the number of shells from 200 to 1000 resulted in changes in the computed oscillation frequencies by less than 1 part in 10^5 for all modes considered.

As a further check on the accuracy of the computed frequencies, we evaluated the variational form of the eigenfrequency after convergence using the computed eigenfunctions. We obtained the variational form by integrating the radial weight functions, as described by Cox (1980). Agreement between the integrated frequency and the eigenfrequency was always closer than 1 part in 10^4, with the agreement being closest for lower overtones. Since these weight functions result

from asymptotic solution to the linear adiabatic wave equation, one would expect to obtain closer agreement for the high overtones. However, the integration of the weight functions was performed as a side calculation to the evaluation of the true eigenfrequency. The step size in the Runge-Kutta integration was set by the shape of the eigenfunctions and not the weight function. To adequately sample the weight function would require a different zoning strategy, and so the integrated frequency of the higher overtone modes was adversely affected at the expense of accurate eigenfunction shapes. In any case, the agreement between the integrated frequency and the eigenfrequency is more than adequate for the purposes of this paper.

3.2. *Nonadiabatic Pulsation Computation*

As discussed in Cox (1980), inward shooting techniques for solving the differential equations describing linear, radial *non*-adiabatic oscillations diverge rapidly while still in the surface layers. Hence we were forced to abandon the Runge-Kutta technique to calculate the nonadiabatic properties of the models. Instead, we used the Newton-Rapheson technique to solve for the eigenfunctions and eigenvalues. The solution technique is similar to that described in SWR, but with a few simplifications. In this study, we ignore the contribution of perturbations of the radiation pressure to the equations. Also, in deriving the equations, SWR assumed a form for J, the specific intensity, that includes the gravitational energy term. In this study, we ignore this term as well. For instance, equation (A3) of SWR is replaced in this study with

$$\lambda_T \frac{d(\delta s/c_p)}{dr} = -b_1 \frac{\delta P}{P} + \left[(4-\kappa_T) + \kappa_\rho \frac{\chi_T}{\chi_\rho}\right]\frac{\delta s}{c_p} + \left[2\left(1+\frac{1}{f}\right) - \alpha(C_1\omega^2+4)\right]\frac{\delta r}{r} - \frac{\delta L_r}{L_r}, \quad (2)$$

where all physical quantities are as defined in SWR. In this and the remainder of the equations we follow the usual convention denoting the Lagrangian variation of a quantity x by δx. The remaining modifications to the SWR equations are equivalent to ignoring all terms proportional to Θ. For example, the nonadiabatic outer boundary condition that enforces the assumption of no inward flux at the outer boundary becomes

$$\nabla_{\rm ad}\frac{\delta P}{P} + \frac{1}{2}\frac{\delta r}{r} + \frac{\delta s}{c_p} - \frac{1}{4}\frac{\delta L}{L} = 0\,. \quad (3)$$

This equation, along with the adiabatic surface boundary conditions, are the three outer boundary conditions. We use a slightly different form than SWR for the inner boundary conditions as well. To obtain regular solutions our central boundary conditions ensure that the spatial derivatives of $\delta r/r$ and $\delta L/L$ vanish at the center. None of these simplifications had any significant effect on the outcome of the computations.

The nonadiabatic calculations produce complex eigenfrequencies for the spectrum of radial modes. The real part of the eigenvalue corresponds to the pulsation frequency and is normally within 1% of the adiabatic frequency. The imaginary part of the eigenfrequency corresponds to the damping rate for the oscillations. For convenience, let us define the negative of the imaginary part of the eigenvalue as κ, the linear "growth rate." Thus $1/\kappa$ represents the e-folding time for the amplitude of the mode. The growth rate is negative for modes that are stable, and positive for linearly unstable modes.

Because the relaxation solution to the nonadiabatic equations is limited in spatial resolution to the zoning of the input equilibrium model, the precision of the nonadiabatic eigenvalues is not as high as the adiabatic values determined as described in the previous section. As discussed in SWR, the models underresolve the eigenfunctions, resulting in an underestimate of the number of radial nodes. However, the eigenvalues are at least representative of the ideal values. More precisely, we find that the period of the first and last unstable radial modes is largely independent of the zoning. For the ML2 model at 30,000 K containing 600 zones, the first unstable mode has a period of 0.577 s ($k = 23$), and the last unstable mode has a period of 0.122 s ($k = 104$). These k values are determined using the eigenfunction values at the grid points only; the trye value of k could be greater than this, especially for higher order modes. These periods can be compared with the periods determined using a model with the same parameters, but only about 310 shells: the first unstable mode has a period of 0.567 s ($k = 23$) and the last unstable mode has a period of 0.123 s ($k = 87$). Note that the periods in these two models are very close for these important modes, but that the eigenfunctions are seriously underresolved in the 310 zone model. We note here that the mode with a period closest to 0.122 s has a value of k that is 119, as determined using the adiabatic code. Thus the nonadiabatic code, using the model with 600 zones, is missing approximately 15 interior nodes.

The growth rates as a function of period also depend only slightly on the coarseness of the zoning in the models. The maximum difference in the growth rate is only 40%, with the coarsely zoned model having somewhat greater growth rates. For the purposes of this study, we are mainly concerned only with the sign and the order of magnitude of the growth rate. Since the growth rates in the models are in general only believable to a factor of 2 or so, this small difference between models with different zonings is not significant. Hence we use the adiabatic radial code to determine accurate periods for the models, and the nonadiabatic pulsation code to determine the stability and growth rate as a function of period for the same model.

We also note here that the high-overtone radial modes have frequencies that are shorter than 0.1 s for k greater than about 110. At these short periods, which approach the acoustic cutoff frequency, the surface boundary condition begins to break down. Modes with shorter periods than the cutoff period do not see the surface of the star as reflective; energy pumped into such modes escapes through the surface as a running wave. The cutoff period for DB white dwarf models is approximately 0.08 to 0.10 s (Hansen, Winget, & Kawaler 1985). Therefore the leakage of energy through the photosphere limits the linearly unstable periods to longer than about 0.08–0.10 s.

3.3. *Asymptotic Relations*

The computational resources required to compute the accurate pulsation periods for higher order radial pulsations are nontrivial. However, as k increases, the eigenfrequencies approach values that are easily computed using the asymptotic behavior of the linear adiabatic wave equation. Following the analysis of Tassoul & Tassoul (1968) the wave equation can be expressed in the form

$$\frac{d^2w}{dr^2} + w\left[\frac{\sigma^2}{c_s^2} - \phi(r)\right] = 0\,, \quad (4)$$

where c_s is the adiabatic sound speed, w is the "wave function," and $\phi(r)$ is a depth-dependent function of the structural param-

eters of the equilibrium model. The wave function w is oscillatory as long as the factor in brackets in the above equation is greater than zero; that is, the eigenfunction is oscillatory when $\sigma^2 > c_s^2\phi$. When this condition holds, the solution to the wave equation is of the form

$$w(r) \propto e^{ik_r r} , \tag{5}$$

where

$$k_r^2 = \frac{\sigma^2}{c_s^2} - \phi(r) \tag{6}$$

is the radial wave number for the mode at position r. For an oscillatory solution, an integral number of half-wavelengths of the eigenfunction must fit between the turning points. If the eigenfunction changes much more quickly than the function $\phi(r)$, then we obtain the eigenvalue condition

$$\int_a^b k_r\, dr = (n + 1)\pi , \tag{7}$$

where n is the number of nodes in the eigenfunction, and the integral is over the regions where the eigenfunction is oscillatory. An illustrative example is for high-frequency (and therefore high-overtone) modes, where $\sigma^2 \gg c_s^2\phi$. In this case we can write

$$\nu_n = \nu_0(n + 1) , \tag{8}$$

where

$$\nu_0 = \frac{1}{2}\left(\int_a^b \frac{dr}{c_s}\right)^{-1} \propto \sqrt{G\langle\rho\rangle} , \tag{9}$$

where the last expression is merely the period-mean density relation. Thus in the high-frequency limit, the frequencies of radial modes become equally spaced in frequency, with the spacing equal to ν_0. This well-known result allows us to ensure that the numerical solution of the pulsation equations produce eigenfrequencies that are accurate and consistent. We show in the next section how this equation can provide a mass determination in radially pulsating white dwarfs.

4. ADIABATIC FREQUENCIES

The computed frequencies of our models follow the expectations based on asymptotic analysis. As an illustration, we show in Figure 2 the frequency separation between successive modes as a function of n in a 0.60 $M_\odot$ model (T_e = 25,000, ML2). The frequency difference approaches the constant value ν_0 with increasing frequency. As n increases, the local wavenumber decreases in comparison to the scale over which $\phi(r)$ changes, and the WKB conditions are approached. In fact, the frequency of the n = 140 mode is approximately 10 s^{-1}, so that departures of the frequencies from their asymptotic limits are much less than 1 part in 10^4. The adiabatic Runge-Kutta code produces very reliable frequencies and mode identifications, with an expected precision of about 1 part in 10^5. Also shown in Figure 2 is the result for the frequencies of this model computed with the nonadiabatic relaxation code. The poor resolution of the high-order eigenfunctions results in relatively large departures from uniform frequency spacing, as expected.

Note also that at this level there is oscillatory behavior in Figure 2. This real effect is caused by discontinuous change in $\phi(r)$ across the helium-carbon composition boundary and can be understood analytically (Gough 1990). If these modes are indeed observed, and the needed precision of the frequency measurements achieved, radial modes could in principle provide a measurement of the depth of the surface helium layer, in a way that is complementary to the successful mode-trapping studies of nonradial oscillations in DB and DA white dwarfs (Kawaler & Weiss 1990; Bradley & Winget 1991; Bradley, Winget, & Wood 1992; Brassard et al. 1992).

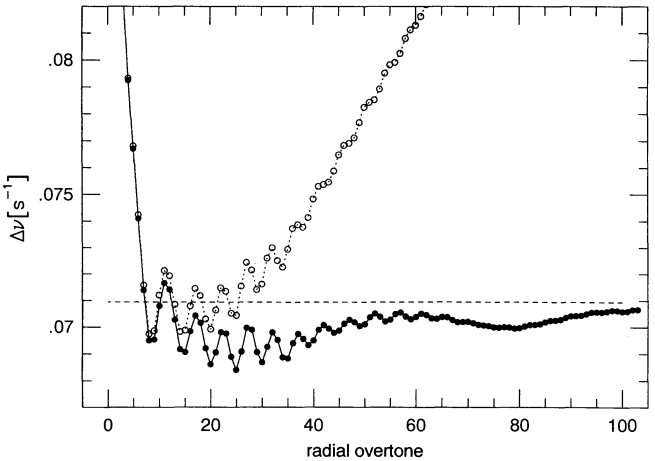

FIG. 2.—Difference in frequency between successive radial overtones as a function of overtone for two types of adiabatic pulsation calculations. The equilibrium model is 0.60 $M_\odot$, T_e = 25,000 K, using ML2 convection. The solid line connects modes computed using a shooting technique that fully resolves all eigenfunctions. The dotted line connects modes computed using a relaxation technique that solves for the eigenfunctions on the input model grid. The dashed line is at a fixed frequency difference corresponding to the asymptotic solution in the limit of high radial overtone. Clearly the relaxation technique grossly underresolves the node number for a given frequency. Note that the wiggles in the solid curves are real, and result from a slight degree of mode trapping in radial modes by the helium/carbon composition transition zone.

The uniform frequency spacing seen for high-order radial modes holds the key to detecting these modes in observations of DB white dwarfs. As we will soon see, many modes are unstable in these models, so that if they are excited to high enough amplitude, these stars should be multiperiodic. The amplitude of individual modes may indeed be quite low and not easily distinguished from noise. However, the noise peaks in a power spectrum should be at random frequencies, while the peaks due to radial pulsation are uniformly spaced in frequency. Thus one can increase the chances of detection by looking for correlations in the frequencies of peaks in the power spectrum. One technique to uncover the modes would be to perform a Fourier transform of the power spectrum. Radial modes would be responsible for a peak in this Fourier transform of the Fourier transform (FT^2) at a frequency of $1/\nu_0$, or about 14 Hz^{-1}. We strongly recommend this approach to searches for radial oscillations in white dwarfs and demonstrate the technique in the final section of this paper.

Table 1 presents the values of ν_0 for various 0.60 $M_\odot$ models. These values were computed by integrating the inverse of the sound speed through the model and agree to better than 1 part in 10^3 with the computed values of the high-overtone radial oscillation modes. Note that for all of the 0.60 $M_\odot$ models $\nu_0 \simeq 0.070$ s^{-1}, and that at a given value of T_e, ν_0 is insensitive to the efficiency of convection.

The asymptotic analysis above indicates that ν_0 scales as $(M/R^3)^{1/2}$. This scaling controls the dependence of ν_0 on T_e and stellar mass. The increase of ν_0 with decreasing effective temperature (and therefore decreasing radius) is a result of the

TABLE 1

ASYMPTOTIC FREQUENCY SPACING (v_0)[a]

$T_{\rm eff}$	ML1	ML2	ML3
19,000.....	0.07420	...	...
20,000.....	0.07357	...	...
21,000.....	0.07297	...	...
22,000.....	0.07240	0.07267	...
23,000.....	0.07185	0.07209	...
24,000.....	0.07131	0.07151	...
25,000.....	0.07078	0.07094	...
26,000.....	0.07027	0.07038	0.07056
27,000.....	0.06976	0.06983	0.07001
28,000.....	0.06925	0.06929	0.06945
29,000.....	0.06875	0.06877	0.06889
29,500.....	0.06850	...	...
30,000.....	0.06825	0.06826	0.06833
31,000.....	0.06775	0.06775	0.06777
31,500.....	...	0.06750	0.06751
31,750.....	...	...	0.06738
32,000.....	0.06724	0.06725	0.06725

[a] In cycles s^{-1} for 0.60 $M_\odot$ DB models.

models' approach to the zero-temperature mass-radius relation. As mass increases, v_0 increases as well: Table 2 shows the structural properties of DB white dwarf models of different mass, but all with $T_e = 25{,}000$ K, and ML2 convection. Because these models all lie close to the zero-temperature mass-radius relation, the radius is a function only of the stellar mass. In the limited mass range of interest for white dwarfs, we find that our model radii scale as $R \propto M^{-0.8}$. Therefore, from Table 2, we can derive a relationship between v_0 and stellar mass

$$v_0 = 0.171\left(\frac{M}{M_\odot}\right)^{1.7}. \quad (10)$$

While derived for models at a single effective temperature, the approximate nature of this relation renders it independent of the small dependence of v_0 on T_e. It is easy to see that if multimode high-overtone radial pulsations are observed in DB white dwarfs, then the observed frequency distibution will allow precise determination of the mass of the star.

5. NONADIABATIC RESULTS

5.1. *The Blue Edge and Convective Efficiency*

DB white dwarf models are linearly unstable to radial pulsations soon after they develop surface convection zones; this occurs at effective temperatures around 31,000 K. As a DB white dwarf cools below 35,000 K, the conditions in the outermost layers allow recombination of He II. This recombination results in large opacities which in turn block the radiative flux to the point where the outer layers become convectively unstable. As the star cools further, partial ionization and the associated convection is driven deeper into the star. At some point, the thermal time scale in the surface convection zone reaches a few tenths of a second, which is similar to the periods of high-overtone radial pulsation modes. Therefore, the well-known κ and γ effects can operate to destabilize these high-order radial modes.

The theoretical blue edge for radial pulsation lies at about 31,000 K in our models, with a weak dependence on the efficiency of convection. Table 3 lists the blue edges found for three model sequences for both the radial and nonradial modes. In all cases, the initial unstable modes have periods between 0.14 and 0.22 s. As the models cool below the blue edge, the period of the lowest overtone unstable mode rapidly reaches the radial fundamental of approximately 12 s, while the shortest unstable period drops to below the acoustic cutoff period. For yet cooler models, the degree of the highest unstable overtone gradually diminishes.

Note that while more efficient convection gives a somewhat bluer radial blue edge, the blue edge varies by less than 2500 K from ML1 through ML3. For nonradial modes, however, the blue edge is much more sensitive to the treatment of surface convection, increasing 8500 K from ML1 through ML3. Therefore, the difference between the radial and nonradial blue edge increases substantially with decreasing convective efficiency. This is consistent with the conclusions drawn earlier from Figure 1, as the thermal time scale at the base of the convection zone increases faster with decreasing temperature for models with efficient convection. Thus an observational determination of the blue edge for radial pulsations can help confirm the suggestion from nonradial studies that convection is very efficient in DB white dwarfs. This conclusion generalizes to DA white dwarfs as well (see § 6 below).

5.2. *Growth Rates for Unstable Modes*

For a given model, the growth rate is largest for the shortest period modes, with the low overtones having the longest growth times. In Figure 3 we show the growth rate as a function of period for several models in the ML2 sequence. These plots are qualitatively similar to those for DA models presented by SWR. This should come as no surprise because of the structural similarity between DA and DB white dwarf models, and in the driving mechanism. As discussed by SWR, the shapes of these curves can be understood in terms of the time scales with the partial ionization zone. In the models, some radiative damping occurs above the driving region. Modes with periods significantly shorter than $\tau_{\rm bc}$ will be damped more than the slightly longer period modes; this is because these modes have small amplitudes in the surface driving zone. Similarly, modes with periods significantly longer than $\tau_{\rm bc}$ will have

TABLE 2

MASS DEPENDENCE OF STRUCTURAL PROPERTIES OF DB WHITE DWARF MODELS

$M/M_\odot$	$\log (R/R_\odot)$	$\log (L/L_\odot)$	v_0
0.40.....	−1.7721	−1.0010	0.03591
0.50.....	−1.8451	−1.1469	0.05242
0.55.....	−1.8753	−1.2073	0.06137
0.60.....	−1.9033	−1.2633	0.07094
0.65.....	−1.9299	−1.3166	0.08129
0.70.....	−1.9558	−1.3684	0.09256
0.80.....	−2.0073	−1.4714	0.11879

NOTE.—All models have $T_e = 25{,}000$ K and use the ML2 prescription for convection.

TABLE 3

EFFECTIVE TEMPERATURE FOR RADIAL AND NONRADIAL BLUE EDGE IN 0.60 $M_\odot$ DB MODELS

	ML1	ML2	ML3
Radial	29500	31000	31750
Nonradial	20000	25500	28500
$\theta (= T_r - T_{nr})$	9500	5500	3250

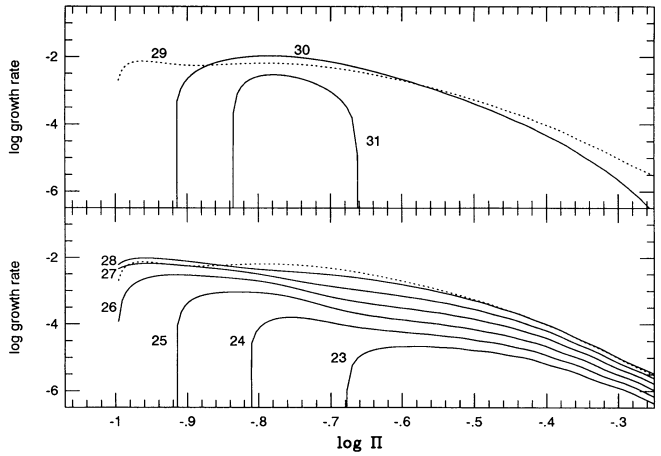

FIG. 3.—Growth rate (in s^{-1}) as a function of pulsation period for radial modes in the ML2 sequence. The curves join modes for a model with the effective temperature (in units of 1000 K) indicated. The upper panel shows growth rates for models near the blue edge, while the lower panel displays models at lower effective temperatures. The dashed line is the growth rate curve for the model at 29,000 K; it is repeated in the bottom panel for comparison purposes.

smaller growth rates as the partial ionization zone adjusts quickly (and therefore more adiabatically) to oscillations on those longer time scales. For these longer period modes, the eigenfunctions have significant amplitude in the damping region below the surface convection zone. Thus the driving is greatest for modes with periods at (or slightly shorter than) τ_{bc}, and diminished on either side of that period.

Some properties of driving near the blue edge are illustrated in Figure 4. This figure illustrates that radial instability near the blue edge is a classic example of driving by the κ and γ mechanisms working together. Figure 4 shows the integrated work function along with κ_T (the logarithmic derivative of the opacity with respect to temperature at constant density) and $\Gamma_3 - 1$ (the logarithmic derivative of temperature with respect to density at constant entropy). Areas of driving can be identified as regions where the integrated work increases outward. For this choice of abscissa, the surface (defined as $\tau = 10^{-3}$) lies at the left, and the center toward the right. The model in Figure 4 was computed using ML2 convection at $T_e = 30{,}000$ K; therefore it is near the blue edge. The second panel shows the integrated work function for the $n = 80$ mode, with a period of 0.166 s and a growth rate of $+1.07 \times 10^{-2}\ s^{-1}$, this mode is unstable. The top panel shows the work function for the stable $n = 10$ mode, with a period of 1.185 s and a growth rate of $-1.22 \times 10^{-9}\ s^{-1}$. In this model the peak driving occurs at $\log(1 - r/R) = -4.0$, below the top of the convection zone at $\log(1 - r/R) = -4.4$. The photosphere lies at $\log(1 - r/R) = -4.36$. Damping is greatest at and below the base of the convection zone, which lies at $\log(1 - r/R) = -3.85$ in this model. Clearly, in this model, the driving is via the $(\kappa - \gamma)$ mechanisms, as the peak lies at the minimum in $\Gamma_3 - 1$, while κ_T is about -2 (see Cox 1980).

Figure 5 illustrates further the physics behind the range of unstable periods. The pressure perturbation eigenfunction for three modes are shown on a common scale; note that the higher the overtone, the shallower the penetration of the eigenfunction into the inner layers of the star. For the stable $n = 20$ mode, the eigenfunction penetrates well below the convection zone. Thus this mode is damped by the white dwarf core. For

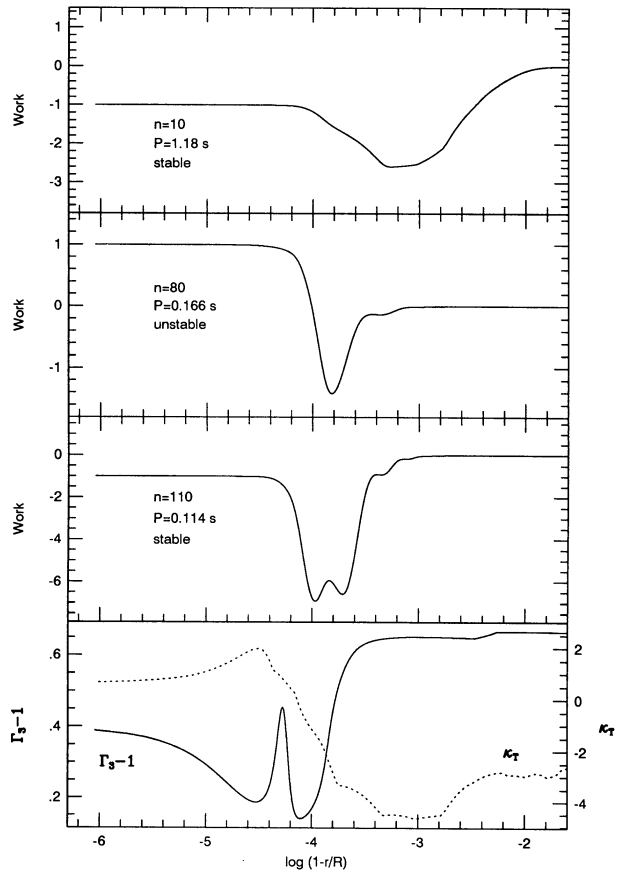

FIG. 4.—Work functions and physical quantities for the 30,000 K model from the 0.60 $M_\odot$ ML2 sequence. The abscissa is the logarithm of the surface radius fraction; thus the surface lies to the left in this figure, the center lies beyond the right edge at zero. The bottom panel shows the values of $\Gamma_3 - 1$ and κ_T in the outer layers of the model. The three top panels show the integrated work function (normalized to the surface value) for the indicated modes.

the unstable mode with $n = 80$, the eigenfunction is nearly zero below the convection zone and increases through the driving zone. The stable $n = 110$ mode does not penetrate significantly below the photosphere, and so driving of that mode by the

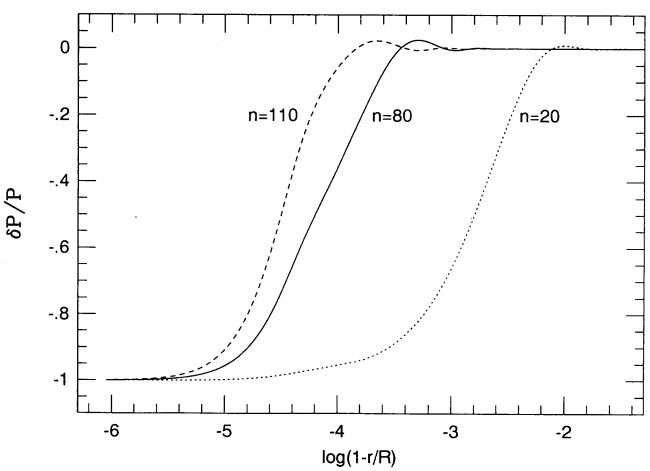

FIG. 5.—Pressure perturbation eigenfunctions for the indicated modes in the 30,000 K model from the 0.60 $M_\odot$ ML2 sequence. The eigenfunctions have been normalized to their surface values.

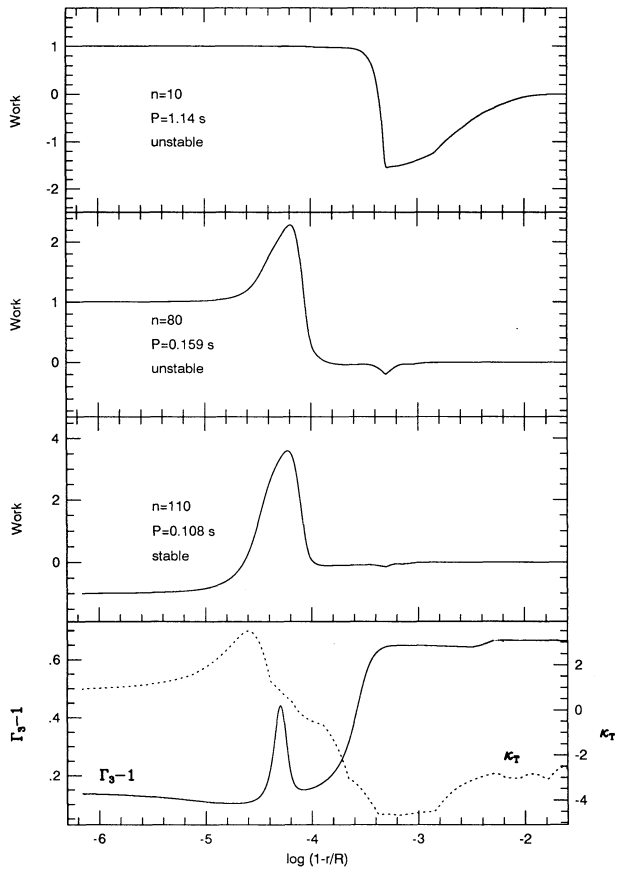

FIG. 6.—Same as Fig. 4, but for the 25,000 K model from the ML2 sequence. Note that the integrated work decreases outward for the $n = 80$ and $n = 110$ modes, indicating damping near the photosphere.

convection zone is not great enough to overcome the near-surface damping.

Well within the blue edge, the nonadiabatic properties of the modes are somewhat different. Figure 6 is the same as Figure 4, but for a model at 25,000 K. In this model, the top of the convection zone lies at $\log (1 - r/R) = -4.59$, the photosphere is at $\log (1 - r/R) = -4.49$, and the base of the convection zone is at $\log (1 - r/R) = -3.30$. The work function again shows driving at a point near the top of the convection zone, with a local maximum at $\log (1 - r/R) = -4.08$. However, there is quite a bit of action right at the base of the convection zone for the lower overtone modes. As discussed in SWR, driving within the partial ionization zone is reduced, in a relative sense, where convection carries a significant fraction of the total flux. In this model, convection is very efficient in the middle of the convection zone, and therefore the radiative flux, and its perturbation, is quite small. This accounts in part for the flat part of the integrated work function between $\log (1 - r/R) = -3.5$ and -3.8. The reduction in the driving results in the lower growth rates for the longer period overtones and is responsible for the shoulder in the growth rate versus period relation in Figure 3 that develops below about 29,000 K.

As the star cools, the partial ionization region works its way deeper, into regions with longer thermal time scales. As the above arguments suggest, the period of the most unstable modes should increase with decreasing T_e. Table 4 lists the most unstable mode for several models. The general trend is for the period of the most unstable mode to increase. Note also that the growth rate for the most unstable mode reaches a maximum about 1500 K to 2000 K inside the blue edge. However, near the blue edge, the period of the most unstable mode in the ML2 and ML3 sequences actually decreases discontinuously as the model cools through the first 2000 K or so below the blue edge. This is because of the double-humped shape of the growth rate as a function of n; as the smaller n bump decays, the period of the most unstable mode switches to the larger n bump. The maximum growth rate reached in a given sequence is roughly 10^{-2} s^{-1}, corresponding to a growth time of about 100 s.

6. CONCLUSIONS

These calculations, which confirm and expand upon earlier studies, are quite robust in their prediction that DB white dwarfs between about 25,000 K and 31,000 K are unstable against radial pulsation. There have as yet been no published studies of the photometric properties of DB white dwarf stars

TABLE 4

UNSTABLE MODES WITH LARGEST GROWTH RATES FOR 0.60 $M_\odot$ MODELS

	ML1		ML2		ML3	
$T_{\rm eff}$	$P_{\rm max}(k_{\rm max})$	$\kappa_{\rm max}$	$P_{\rm max}(k_{\rm max})$	$\kappa_{\rm max}$	$P_{\rm max}(k_{\rm max})$	$\kappa_{\rm max}$
19,000.....	0.280 (45)	1.45×10^{-5}	...	...	...	...
20,000.....	0.254 (50)	4.96×10^{-5}	...	...	...	...
21,000.....	0.223 (57)	1.65×10^{-4}	...	...	...	...
22,000.....	0.210 (61)	4.22×10^{-4}	0.292 (44)	8.37×10^{-6}	...	...
23,000.....	0.194 (66)	8.01×10^{-4}	0.264 (49)	2.17×10^{-5}	...	...
24,000.....	0.186 (69)	1.24×10^{-3}	0.172 (72)	1.63×10^{-4}	...	...
25,000.....	0.174 (74)	2.97×10^{-3}	0.150 (84)	9.22×10^{-4}	...	...
26,000.....	0.163 (79)	5.35×10^{-3}	0.122 (101)	3.01×10^{-3}	0.136 (92)	2.68×10^{-3}
27,000.....	0.160 (81)	7.00×10^{-3}	0.110 (110)	6.63×10^{-3}	0.109 (111)	7.83×10^{-3}
28,000.....	0.159 (82)	7.00×10^{-3}	0.110 (111)	9.67×10^{-3}	0.109 (112)	1.13×10^{-2}
29,000.....	0.160 (82)	4.64×10^{-3}	0.109 (113)	7.39×10^{-3}	0.112 (110)	1.68×10^{-2}
29,500.....	0.163 (81)	2.46×10^{-3}	...	...	...	...
30,000.....	Stable	Stable	0.164 (81)	1.07×10^{-2}	0.112 (111)	2.00×10^{-2}
31,000.....	Stable	Stable	0.167 (80)	2.93×10^{-3}	0.112 (112)	1.45×10^{-2}
31,500.....	Stable	Stable	Stable	Stable	0.171 (79)	1.28×10^{-2}
31,750.....	Stable	Stable	Stable	Stable	0.169 (80)	6.95×10^{-3}
32,000.....	Stable	Stable	Stable	Stable	Stable	Stable

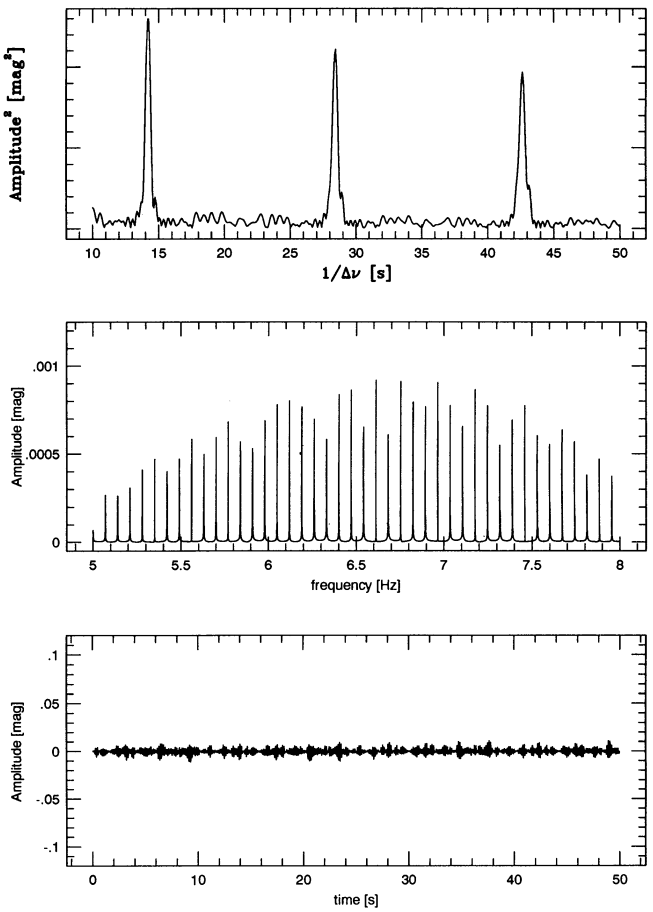

FIG. 7.—Analysis of simulated radial pulsations in a DB model, with input fractional amplitudes of modes equal in magnitude to the growth rates. The bottom panel shows a 50 s segment of the "light curve"; the entire run is 1600 s. The middle panel shows a segment of the Fourier transform of the entire time series. The top panel is a Fourier transform of the Fourier transform (FT^2) and shows peaks at the inverse of the input frequency spacing (14.2 s) its first and second harmonics (28.4 s and 42.6 s).

with the very high time resolution required to detect the high-overtone radial modes.

6.1. *A Search Strategy*

The observational approach described in SWR and Robinson (1984) involves examination of individual peaks in the power spectra of white dwarf stars for statistical significance. While a large-amplitude peak in the power spectrum would be conclusive evidence for radial pulsation, the observations showed no such peaks. Upper limits are quoted for several stars and ranged from 0.5 to 2 mmag for the ZZ Ceti stars that were studied. That is, there were no significant peaks at those levels in any of the stars.

The theoretical models suggest that these stars should be multiperiodic since the growth rates for the high-order modes are all comparable. Based on these growth rates, one would expect dozens of modes to be present with periods between 0.1 and 0.5 s. Furthermore, these high-overtone modes should be equally spaced in frequency. While individual modes might be buried in the noise, we can in principle use their constant frequency spacing to try to dig them out of the noise. Since the noise in the data comes from photon counting statistics coupled with scintillation noise, the distribution of noise peaks in the Fourier transform should be uncorrelated. However, the peaks caused by radial pulsations will occur at a fixed frequency interval. Therefore, the Fourier transform itself should be searched for low-amplitude peaks that are equally spaced.

Such a coherent spacing of spectral peaks could only be caused by radial pulsations. Therefore, we can in principle dig the signal of radial pulsations out of the observed power spectrum by correlating the power spectrum with a "picket fence" of equally spaced delta functions. The correlation value will reach a maximum when the spacing of the pickets equals the spacing in frequency of the radial modes. Equivalently, one can take the Fourier transform of the power spectrum. This will produce a peak at the inverse of the frequency spacing. The nonsinusoidal shape of the power spectrum peaks will result in integral harmonics of the principal spacing in the FT^2. These harmonics can be used for verification of existence of the principal spacing.

As an example of how this works, we have synthesized photometric data for a radially pulsating DB white dwarf in Figures 7 and 8. Figure 7 shows the light curve, power spectrum, and FT^2 for data synthesized using the results for the ML2 model at 25,000 K, with no noise. The amplitudes of the modes are set equal to their growth rates for illustration pur-

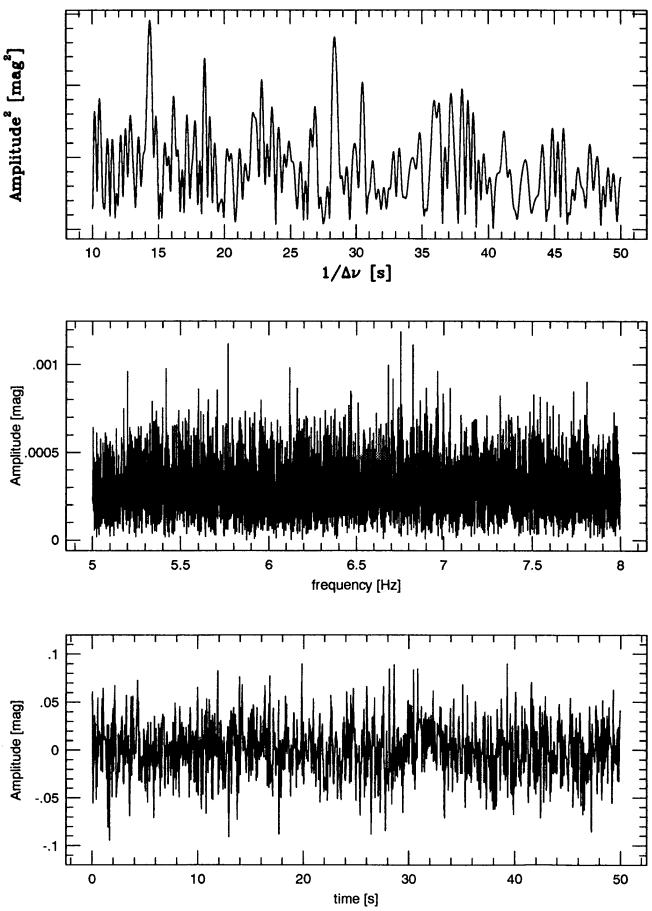

FIG. 8.—Same as Fig. 7, but with the inclusion of Poisson noise appropriate for 1100 counts per 0.05 s integration; the run length is again 1600 s. No significant peaks can be readily identified in the Fourier transform, yet the FT^2 still shows a significant peak at the inverse of the input frequency spacing (14.2 s) its first harmonic (28.4 s).

poses. Clearly, the Fourier transform shows the input frequencies and their amplitudes. The FT^2 shows a correlation peak at precisely the inverse of ν_0, and at its higher harmonics. Figure 8 shows the same synthetic data, but with Poisson noise added at amplitude appropriate to representative count rates for white dwarf stars. With a count rate of 1100 counts per 0.05 integration, the amplitude uncertainty per bin is 30 mmag, significantly larger than the input signal. In the 1600 s duration of this simulated run, however, the amplitude uncertainty is 0.17 mmag. In the Fourier transform, only a few modes peak above the noise level. Yet the FT^2 shows a clear peak at $1/\nu_0$ and it first harmonic. Thus a signal is indeed recovered from the synthetic data, even though examination of the power spectrum shows no conclusive peaks.

6.2. *Where Are the Radially Pulsating White Dwarfs?*

Similar theoretical results reported for DA white dwarfs by a number of authors (SWR and references therein) led to observational searches for radial pulsations in DA white dwarfs. Robinson (1984) summarizes several search efforts for such pulsations, none of which detected the predicted pulsations. The upper limits quoted in Robinson (1984) all lie at about the millimagnitude level, with shortest detectable periods of 0.2 s. This failure to detect the predicted pulsations poses a significant challenge to pulsation theory, as the predictions are based on the same physics and modeling techniques that have so successfully described the pulsations of a wide variety of variable stars ranging from Mira variables to the Cepheids and the ZZ Ceti stars. Numerous suggested explanations have been proposed to explain away the pulsations, including attempts to invoke the convection-pulsation interaction (i.e., Starrfield & Cox 1989) which is normally ignored in pulsation studies.

However, there are at least two ways that the observational efforts could have missed detecting the pulsations. First, the most unstable modes could have periods that are at or above the Nyquist frequency. Second, the chosen candidate objects may not represent the best possible objects for visibility of the high-overtone modes.

To examine these possibilities, we produced a sequence of DA white dwarf models using the structure code described earlier. This 0.60 $M_\odot$ pilot sequence had a surface helium layer of 10^{-4} stellar masses, and a surface hydrogen layer of 10^{-10} stellar masses. The ML3 convection formalism was employed, but the mixing length was not reduced near the top of the convection zone. The nonradial blue edge for this sequence is at about 12,700 K, in fair agreement with the observed value of 13,000 K (Wesemael et al. 1991). These models show a radial blue edge at about 13,600 K, or roughly 900 K hotter than the nonradial instability strip. These results for an ML3 sequence are not consistent with SWR's suggestion that the temperature difference between the radial and nonradial blue edges is independent of the efficiency of convection. They found a temperature difference of 1600 K between the blue edges for their ML1 sequences. The reason for this difference can be seen by examination of the thermal time scale at the base of the surface convection zone, in a way completely analogous to the case for the DB models presented in § 5. That is, in ML3 models, τ_{bc} increases rapidly with decreasing T_e; thus the blue edges for radial and nonradial modes are close together. This increase is less rapid for ML1 models, so that the blue edges are farther apart in T_e than in the ML3 models. This behavior is illustrated very clearly in Figure 9 of Tassoul et al. (1990).

Thus the theoretical blue edge for radial pulsations in DA white dwarfs is redder than assumed by SWR and Robinson (1984), based on the calibration of the mixing length parameterization provided by the observed value of the blue edge of the ZZ Ceti instability strip. With this as the case, the three hottest objects in Robinson (1984) are probably hotter than the blue edge of the radial instability strip and are not expected to pulsate. Of the other objects, those significantly to the red of the blue edge will have smaller growth rates than those nearer the blue edge. Thus the remaining objects that are the best candidates in Robinson (1984) are the three objects near the ZZ Ceti blue edge; G117−B15A, G130−5, and GD 52. Of those, only G117−B15A is a ZZ Ceti star; the others, while within the strip as defined by their $(G-R)$ color, are not nonradial pulsators. Thus either they are just outside the nonradial instability strip, or they are odd in some way. These three stars then are the prime suspects, for they should show radial pulsations yet none has been observed.

The pilot DA model at 13,500 K can help here. This model lies near the nonradial blue edge and is unstable to radial pulsations. The period range for the unstable modes lies between 0.13 and 0.23 s, with the most unstable mode having a period of 0.14 s. For comparison, a DA model at 13,000 K has unstable modes between 0.15 and 3.40 s, with the maximum growth at a period of 0.20 s. While the growth rates we find are somewhat higher than SWR report, the periods of the most unstable modes are comparable to their results. Thus the models suggest that the most promising modes for detection have periods at and below about 0.2 s. However, the Nyquist frequency for two out of the three best candidates from Robinson (1984) is at 0.20 s. Thus searches for these modes in these data become quite complex because of the sampling interval used. The only object with a high enough Nyquist frequency is G130−5. Using the simple technique described below, these data should be re-examined, as they are the best (and only) real test of the theoretical predictions regarding radial pulsations in DA white dwarfs.

In summary, current theoretical models of DB (and DA) white dwarfs suggest that they should be very high frequency multiperiodic pulsators. Observations of the pulsations can in principle provide high-precision mass determinations for these stars. While such pulsations have not been detected yet, the potential impact that discovery of these pulsations would have on studies of white dwarfs, and stars in general, is enormous. DB candidates may soon be examined for radial pulsations with the *Hubble Space Telescope*; additional sensitive and sophisticated ground-based searches for these elusive pulsations are urgently needed.

The initial motivation for this work followed discussions with Howard Bond during a visit to the Space Telescope Science Institute. Additional discussions with Carl Hansen, Don Winget, Lee Anne Willson, Curt Struck-Marcell, and Paul Bradley were extremely helpful. Kurt Rosentrater was a valuable help in constructing the model grids. This work is sponsored in part by NASA grant NAGW-1364 and in part by NSF grant AST-9115213 to Iowa State University.

REFERENCES

Arcoragi, J.-P., & Fontaine, G. 1980, ApJ, 242, 1208
Böhm, K.-H., & Stuckl, E. 1967, Z. Astrophys., 66, 487
Bradley, P., & Winget, D. 1991, ApJS, 75, 463
Bradley, P., Winget, D., & Wood, M. 1992, ApJ, 391, L33
Brassard, P., Fontaine, G., Wesemael, F., & Hansen, C. 1992, ApJS, 80, 369
Cox, A. N., Starrfield, S., Kidman, R., & Pesnell, W. D. 1987, ApJ, 317, 303
Cox, J. P. 1980, Theory of Stellar Pulsation (Princeton: Princeton Univ. Press).
Dziembouski, W., & Koester, D. 1981, A&A, 97, 16
Eggleton, P., Faulkner, J., & Flannery, B. 1973, A&A, 23, 325
Gough, D. O. 1990, in Progress of Seismology of the Sun and Stars, ed. Y. Osaki & H. Shibahashi (Berlin: Springer), 283
Hansen, C. J., Winget, D. E., & Kawaler, S. D. 1985, ApJ, 297, 544
Hubbard, W., & Lampe, M. 1969, ApJS, 18, 297
Iben, I., Jr. 1975, ApJ, 196, 525
Iben, I., Jr., & Tutukov, A. 1984, ApJ, 282, 615
Kawaler, S. D. 1990, in Confrontation between Stellar Pulsation and Evolution, ed. C. Cacciari & G. Clementini (Provo: PASP Conf. Ser., 11), 494
Kawaler, S. D., & Bradley, P. 1993, in preparation
Koester, D., & Schönberner, D. 1986, A&A, 154, 125
Ledoux, P. J., & Sauvenier-Goffin, E. 1950, ApJ, 111, 611
Mestel, L. 1952, MNRAS, 112, 583
Press, W. H., Flannery, B. P., Teukolsky, S. A., & Vetterling, W. T. 1986, Numerical Recipes (Cambridge: Cambridge Univ. Press)
Robinson, E. L. 1984, AJ, 89, 1732
Saio, H., & Cox, J. P. 1980, ApJ, 265, 549
Saio, H., Winget, D. E., & Robinson, E. L. 1983, ApJ, 265, 982 (SWR)
Savedoff, M. P., Van Horn, H. M., & Vila, S. C. 1969, ApJ, 155, 221
Starrfield, S., & Cox, A. N. 1989, in White Dwarfs, ed. G. Wegner (Berlin: Springer), 115
Starrfield, S., Cox, A. N., & Hodson, S. W. 1979, in IAU Colloq. 53, White Dwarfs and Variable Degenerate Stars, ed. H. M. Van Horn & V. Weidemann (Rochester: Univ. of Rochester), 382
Starrfield, S. G., Cox, A. N., Hodson, S. W., & Pesnell, W. D. 1983, ApJ, 268, L27
Tassoul, M., Fontaine, G., & Winget, D. E. 1990, ApJS, 72, 335
Tassoul, M., & Tassoul, J. L. 1968, ApJ, 153, 127
Van Horn, H. 1971, in IAU Symp. 42, White Dwarfs, ed. W. Luyten (Dordrecht: Reidel), 97
Wesemael, F., Bergeron, P., Fontaine, G., & Lamontagne, R. 1991, in White Dwarfs, ed. G. Vauclair & E. Sion (Dordrecht: Kluwer), 159
Winget, D. E. 1988, in IAU Symp. 123, Advances in Helio and Asteroseismology, ed. J. Christensen-Dalsgaard & S. Frandsen (Dordrecht: Reidel), 305
Winget, D. E., Van Horn, H. M., Tassoul, M., Hansen, C. J., & Fontaine, G. 1983, ApJ, 268, L33
Wood, M. A. 1992, ApJ, 386, 539